An International Journal of Optimization and Control: Theories & Applications
ISSN: 2146-0957 eISSN: 2146-5703
Vol.16, No.6, pp.2118-2129 (2026)
https://doi.org/10.36922/IJOCTA026120042

RESEARCH ARTICLE

Solitary wave solutions of a generalized schrödinger equation with kerr nonlinearity

Umar Ishtiaq[1,2,3*], Umair Asghar[4,5], Tayyab Kamran[6,7], Kamyar Hosseini[8,9,10], and Ioan-Lucian Popa[11,12]

[1]Office of Research, Innovation and Commercialization, University of Management and Technology, Lahore, Pakistan
[2]Software Development Department, Biruni University, Istanbul, Turkey
[3]Research Center of Applied Mathematics, Khazar University, Baku, Azerbaijan
[4]Department of Mathematics and Statistics, The University of Lahore, 1-KM Defence Road, Lahore, Pakistan
[5]Department of Computer Engineering, Biruni University, Istanbul, Turkey
[6]Department of Mathematics, Quaid-i-Azam University, Islamabad, Pakistan
[7]Jadara Research Center, Jadara University, Irbid, Jordan
[8]Department of Mathematics, Near East University, Mersin 10, Nicosia, Turkey
[9]Department of Mathematical Sciences, Saveetha School of Engineering, SIMATS, Chennai, Tamilnadu, India
[10]Faculty of Engineering and Natural Sciences, Istanbul Okan University, Istanbul, Turkey
[11]Department of Computing, Mathematics and Electronics, "1 Decembrie 1918" University of Alba Iulia, Alba Iulia, Romania
[12]Faculty of Mathematics and Computer Science, Transilvania University of Brasov, Iuliu Maniu Street 50, Brasov, Romania
umarishtiaq000@gmail.com, Umair.Asghar@math.uol.edu.pk, tkamran@qau.edu.pk, kamyar_hosseini@yahoo.com, lucian.popa@uab.ro

ARTICLE INFO

Article history:
Received: March 17, 2026
Revised: July 21, 2026
Accepted: August 3, 2026
Published Online: September 17, 2026

Keywords:
Kudryashov method
Bright soliton
Optical pulse propagation
Goodness-of-fit analysis
Rank correlation

ABSTRACT

This study investigates a generalized Schrödinger equation that governs the propagation of optical pulses in nonlinear media in the presence of Kerr nonlinearity. Using Kudryashov's generalized method, we reduce the model to a Duffing-type ordinary differential equation whose first integral yields an exact bright-soliton solution. We validate this solution in three complementary ways. The admissible parameter regime is stated explicitly, and the values used in every figure are shown to fall within this regime, ensuring that the plotted solutions are real and physically meaningful. The solution is then recovered via a stable boundary-value integration of the reduced equation, which agrees with the closed form to $R^2 = 1.0000$ and a root-mean-square error of order 10^{-11}. Finally, the dependence of the wave on the Kerr coefficient is characterised quantitatively: rank-correlation analysis reveals that the peak amplitude is a perfectly monotone but nonlinear function of the Kerr coefficient (Spearman $\rho = -1$, Kendall $\tau = -1$, Pearson $r = -0.94$) obeying the exact law $|\mathcal{A}|_{\max} \propto \aleph^{-1/2}$, while the characteristic width is proved to be independent of it. Cramér–von Mises and Anderson–Darling goodness-of-fit tests, together with a cumulative-distribution-function outlier screening, confirm that the numerical samples are statistically consistent with the theoretical model and free of artefacts. A phase-plane portrait, a propagation map and a two-parameter amplitude map further clarify the dynamics. All computations were reproduced in a license-free open-source environment to ensure portability and reproducibility.

CC BY

*Corresponding Author

1. Introduction

Many phenomena across various fields of applied science are governed by nonlinear partial differential equations (NLPDEs).[1–5] These equations arise in nonlinear optics, plasma physics, fluid dynamics, and condensed-matter theory, describing behaviours that no linear model can reproduce; recent studies of the Hirota–Maccari system[3] and improved analytical techniques with chaos-detection tools[5] illustrate the richness of the resulting dynamics. Among the solutions of NLPDEs, solitary waves are of particular interest due to their remarkable stability: they retain their shape and speed even after interaction. Their construction is central to understanding the intrinsic dynamics of nonlinear systems and sheds light on the physical mechanisms underlying observed phenomena. Over the past two decades several effective techniques have been developed for this purpose, including the ansatz method,[6–8] the exponential method,[9–11] and other approaches.[12–15]

The present study examines the following generalized Schrödinger equation (gSE)[16]

$$\iota\frac{\partial \mathcal{A}}{\partial y}+\frac{1}{2}\left(\frac{\partial^2 \mathcal{A}}{\partial x^2}+\frac{\partial^2 \mathcal{A}}{\partial z^2}-\frac{\partial^2 \mathcal{A}}{\partial t^2}\right)+\aleph|\mathcal{A}|^2\mathcal{A}=0, \quad (1)$$

which describes the propagation of optical pulses in nonlinear media. Here $\mathcal{A}(x,y,z,t)$ is the complex envelope, y is the evolution (propagation) variable, the mixed-signature operator $\partial_{xx}+\partial_{zz}-\partial_{tt}$ encodes the balance between transverse diffraction and anomalous temporal dispersion, and $\aleph$ is the Kerr coefficient. This model has attracted recent attention. Kumar *et al.*[17] analysed it via Lie symmetry analysis, reducing the governing equation and constructing a range of soliton-type solutions. Hosseini *et al.*[18] carried out a detailed dynamical study of the gSE, covering bifurcation, chaotic behaviour and sensitivity to initial conditions, and derived soliton solutions describing its nonlinear wave structures.

In 2022, a well-structured analytical method,[19] introduced by N. A. Kudryashov, was used to obtain solitary-wave solutions for a class of nonlinear Schrödinger equations. Hosseini and colleagues later confirmed its versatility on various NLPDEs, including coupled nonlinear Schrödinger equations,[20] the Konno–Oono equation,[21] unstable Schrödinger equations,[22] and Ginzburg–Landau equations.[23] Nevertheless, to the best of our knowledge, the generalized Schrödinger equation with Kerr nonlinearity in the form (1) has not been treated by this method.

It is important to position the present contribution precisely relative to the most closely related recent work. Yasin *et al.*[24] studied a generalized higher-order nonlinear Schrödinger equation of cubic–quintic type,

$$\iota q_x-\frac{\beta_2}{2}q_{tt}+\alpha_1|q|^2q-\iota\frac{\beta_3}{6}q_{ttt}-\frac{\beta_4}{24}q_{tttt} +\alpha_2|q|^4q=0, \quad (2)$$

in a single spatial dimension, applying the modified exponential rational function method to obtain multi-peak solitons and breather-type solutions, along with a conservation-law derivation and linear-stability analysis. Although both works belong to the nonlinear Schrödinger family, they differ in ways that are mathematically substantive and establish the novelty of the present study. (i) **Equation (2)** is (1+1)-dimensional with a single elliptic spatial derivative, whereas (1) is (3+1)-dimensional with the mixed-signature operator $\partial_{xx}+\partial_{zz}-\partial_{tt}$; the reduction of (1) therefore depends on the indefinite quadratic form $\alpha_1^2+\gamma_1^2-\theta_1^2$, whose sign controls the existence of a localized solution and has no analogue in (2). (ii) The cubic–quintic terms $\alpha_1|q|^2q+\alpha_2|q|^4q$ and the third- and fourth-order dispersion β_3,β_4 lead, after reduction, to a fourth-order ordinary differential equation with a sextic effective potential, whereas the pure Kerr law in (1) yields a second-order Duffing-type equation with a quartic potential, so that the balance number here is $N=1$ rather than the larger value forced by the quintic term. (iii) The multi-peak and breather structures of[24] arise from competition between quintic nonlinearity and higher-order dispersion; the present model supports a single-hump bright soliton obtained in closed form through Kudryashov's integral reduction, whose amplitude follows the exact power law $|\mathcal{A}|_{\max}\propto\aleph^{-1/2}$ derived below. (iv) Reference[24] uses the modified exponential rational function method, an ansatz-expansion technique, whereas we use Kudryashov's generalized method, which reduces the problem to a first-order auxiliary equation integrated in quadrature and does not require an integer balance number. In short, the present study is not a re-parameterisation of:[24] it treats a structurally different (higher-dimensional, indefinite-operator, pure-Kerr) equation with a different reduction, obtains a different class of solutions, and adds a quantitative statistical validation that[24] did not report.

The principal novelty of this work therefore lies in (a) the first application of Kudryashov's generalized method to the (3+1)-dimensional generalized Schrödinger equation with Kerr nonlinearity; (b) an explicit statement of the admissible parameter regime, with a demonstration that the

reported solutions are real and physically meaningful with it; and (c) a quantitative, reproducible characterisation of the soliton dynamics, including an amplitude-scaling law, correlation analysis, goodness-of-fit testing, and outlier screening, supported by a phase-plane and parameter-map study, all of which move the analysis well beyond visual inspection of the plots.

The remainder of the paper is organized as follows. Section 2 gives a self-contained account of Kudryashov's generalized method. Section 3 reduces the governing model and constructs its solitary-wave solution, with every step derived explicitly. Section 4 examines the influence of Kerr nonlinearity on the dynamics of the solitary wave under suitable parameter regimes, supported by two- and three-dimensional visualizations and by quantitative statistical validation. Section 5 concludes.

2. Kudryashov's generalized method

This section presents a self-contained account of Kudryashov's generalized method,[19–21] together with the conditions under which each transformation is valid. Suppose that, under a travelling-wave reduction, the governing model (1) can be written as a first-order autonomous ordinary differential equation of the form

$$\mathcal{B}_\delta^2 = \Phi(\mathcal{B})\,\Psi(\mathcal{B}), \qquad \mathcal{B} = \mathcal{B}(\delta), \tag{3}$$

where Φ and Ψ are polynomials in $\mathcal{B}$ and the right-hand side is non-negative on the relevant interval, so that $\mathcal{B}_\delta$ is real. Such a first-order form always exists for the conservative second-order equations considered here: multiplying an equation of the type $\mathcal{B}_{\delta\delta} = F(\mathcal{B})$ by $\mathcal{B}_\delta$ and integrating once yields precisely the energy relation (3).

The method integrates (3) by splitting it into two solvable sub-problems through an auxiliary independent variable ζ. Introduce

$$\mathcal{B}(\delta) = \mathcal{M}(\zeta), \qquad \zeta = \Omega(\delta), \tag{4}$$

where Ω is taken to be monotone, hence invertible, so that the correspondence between δ and ζ is one-to-one. Applying the chain rule to (4) gives

$$\mathcal{B}_\delta = \mathcal{M}_\zeta\,\zeta_\delta. \tag{5}$$

Substituting (4) and (5) into (3) yields

$$\mathcal{M}_\zeta^2\,\zeta_\delta^2 = \Phi(\mathcal{M})\,\Psi(\mathcal{M}). \tag{6}$$

The key step is to assign the factor Φ to the auxiliary variable by imposing

$$\zeta_\delta^2 = \Phi(\mathcal{M}), \tag{7}$$

which is admissible precisely when $\Phi(\mathcal{M}) \geq 0$ over the range of $\mathcal{M}$; this choice fixes the map Ω through the quadrature (9) below. With (7) in force, **Equation (6)** decouples into the amplitude equation

$$\mathcal{M}_\zeta^2 = \Psi(\mathcal{M}), \tag{8}$$

whose right-hand side must likewise be non negative for $\mathcal{M}_\zeta$ to be real. The original variable is then recovered from

$$\delta = \delta_0 + \int \frac{d\zeta}{\sqrt{\Phi(\mathcal{M})}}. \tag{9}$$

Equation (8) is a standard first-order separable equation with a known closed-form solution for polynomial Ψ; substituting that solution into the quadrature (9) and inverting the resulting relation produces the solitary-wave solution of (3). A useful feature of the decomposition (7)–(9) is that the balance number entering $\mathcal{M}(\zeta)$ need not be an integer, which broadens the applicability of the procedure relative to expansion methods that require an integer truncation order.[23]

3. Generalized schrödinger equation and its solitary-wave solution

We now apply the method of Section 2 to the governing **Equation (1)**. To obtain its reduced form, introduce the complex travelling-wave transformation[18]

$$\begin{aligned} \mathcal{A}(x,y,z,t) &= \mathcal{B}(\delta)\,e^{\iota(\alpha_2 x+\beta_2 y+\gamma_2 z-\theta_2 t)}, \\ \delta &= \alpha_1 x+\beta_1 y+\gamma_1 z-\theta_1 t, \end{aligned} \tag{10}$$

where $\mathcal{B}(\delta)$ is a real amplitude, θ_1 is the wave velocity and θ_2 the wave frequency. Writing $\psi = \alpha_2 x+\beta_2 y+\gamma_2 z-\theta_2 t$, the required derivatives are

$$\begin{aligned} \iota\,\mathcal{A}_y &= \big(\iota\,\beta_1\mathcal{B}_\delta - \beta_2\mathcal{B}\big)e^{\iota\psi}, \\ \mathcal{A}_{xx} &= \big(\alpha_1^2\mathcal{B}_{\delta\delta} + 2\iota\,\alpha_1\alpha_2\mathcal{B}_\delta - \alpha_2^2\mathcal{B}\big)e^{\iota\psi}, \\ \mathcal{A}_{zz} &= \big(\gamma_1^2\mathcal{B}_{\delta\delta} + 2\iota\,\gamma_1\gamma_2\mathcal{B}_\delta - \gamma_2^2\mathcal{B}\big)e^{\iota\psi}, \\ \mathcal{A}_{tt} &= \big(\theta_1^2\mathcal{B}_{\delta\delta} + 2\iota\,\theta_1\theta_2\mathcal{B}_\delta - \theta_2^2\mathcal{B}\big)e^{\iota\psi}. \end{aligned} \tag{11}$$

Substituting (11) into (1), using $|\mathcal{A}|^2\mathcal{A} = \mathcal{B}^3 e^{\iota\psi}$, dividing through by $e^{\iota\psi}$ and separating the real and imaginary parts, gives the system

$$\textbf{Im:}\ \big(\alpha_1\alpha_2+\gamma_1\gamma_2-\theta_1\theta_2+\beta_1\big)\frac{d\mathcal{B}(\delta)}{d\delta} = 0, \tag{12}$$

$$\begin{aligned} \textbf{Re:}\ \big(\alpha_1^2+\gamma_1^2-\theta_1^2\big)\frac{d^2\mathcal{B}(\delta)}{d\delta^2} - \big(\alpha_2^2+\gamma_2^2-\theta_2^2 \\ +2\beta_2\big)\mathcal{B}(\delta) + 2\aleph\,\mathcal{B}^3(\delta) = 0. \end{aligned} \tag{13}$$

For a non-constant amplitude ($d\mathcal{B}/d\delta \neq 0$), Eq. (12) forces the bracketed coefficient to vanish, which determines the wave velocity as

$$\theta_1 = \frac{\alpha_1\alpha_2+\gamma_1\gamma_2+\beta_1}{\theta_2}. \tag{14}$$

Dividing (13) by $\alpha_1^2+\gamma_1^2-\theta_1^2$ (assumed nonzero) yields the Duffing-type reduced equation

$$\mathcal{B}_{\delta\delta} - A\,\mathcal{B}(\delta) + B\,\mathcal{B}^3(\delta) = 0, \tag{15}$$

where

$$A = \frac{\alpha_2^2+\gamma_2^2-\theta_2^2+2\beta_2}{\alpha_1^2+\gamma_1^2-\theta_1^2}, B = \frac{2\aleph}{\alpha_1^2+\gamma_1^2-\theta_1^2}. \tag{16}$$

Equation (15) governs the envelope $\mathcal{B}(\delta)$, in which dispersion (through A) and Kerr nonlinearity (through B) compete to set the shape of the solitary wave. To fix the leading-order behaviour we apply the homogeneous-balance principle[25] between the highest-order derivative and the nonlinear term of (15). Writing $\mathcal{B} \sim \delta^{-N}$ near a movable singularity, the term $\mathcal{B}_{\delta\delta}$ scales as $\delta^{-(N+2)}$ and $\mathcal{B}^3$ scales as δ^{-3N}; balancing the two exponents gives $3N = N+2$, hence

$$N = 1. \tag{17}$$

This value fixes the degree of the solitary wave. Multiplying (15) by $\mathcal{B}_\delta$ and integrating once (the integration constant vanishes for a wave that decays at infinity) gives the first integral

$$\mathcal{B}_\delta^2 - A\,\mathcal{B}^2(\delta) + \tfrac{1}{2}B\,\mathcal{B}^4(\delta) = 0, \tag{18}$$

which is of the form (3) with $\Phi(\mathcal{B}) = \mathcal{B}^2$ and $\Psi(\mathcal{B}) = A - \frac{1}{2}B\,\mathcal{B}^2$. Introducing the auxiliary variable

$$\mathcal{B}(\delta) = \mathcal{M}(\zeta), \qquad \zeta = \Omega(\delta), \tag{19}$$

and applying the chain rule, $\mathcal{B}_\delta = \mathcal{M}_\zeta \zeta_\delta$, turns (18) into

$$\mathcal{M}_\zeta^2\,\zeta_\delta^2 = A\,\mathcal{M}^2 - \tfrac{1}{2}B\,\mathcal{M}^4. \tag{20}$$

Assigning Φ to the auxiliary variable through $\zeta_\delta = \mathcal{M}(\zeta)$ (admissible since $\Phi = \mathcal{M}^2 \geq 0$), **Equation (20)** decouples into

$$\mathcal{M}_\zeta^2 = A - \tfrac{1}{2}B\,\mathcal{M}^2. \tag{21}$$

The separable equation (21) integrates to

$$\mathcal{B}(\delta) = \mathcal{M}(\zeta) = \sqrt{\frac{2A}{B}}\,\sin\left(\frac{\sqrt{2B}}{2}\,(\zeta_0-\zeta)\right), \tag{22}$$

with ζ_0 an arbitrary constant. For this expression, and for every quantity derived from it, to be real, the coefficients must satisfy

$$A > 0, \qquad B > 0, \tag{23}$$

so that both $\sqrt{2A/B}$ and $\sqrt{2B}$ are real. By (16), the two conditions (23) hold together whenever $\alpha_2^2+\gamma_2^2-\theta_2^2+2\beta_2$ and $\aleph$ share the sign of $\alpha_1^2+\gamma_1^2-\theta_1^2$; this delimits the admissible parameter regime, verified explicitly for the figures in Section 4. Recovering δ from the quadrature (9) with $\Phi = \mathcal{M}^2$ gives

$$\delta = \delta_0 + \int \frac{d\zeta}{\mathcal{M}(\zeta)} = \delta_0 - \frac{\ln\Big(\csc\Big(\frac{\sqrt{2B}}{2}\,(\zeta-\zeta_0)\Big) - \cot\Big(\frac{\sqrt{2B}}{2}\,(\zeta-\zeta_0)\Big)\Big)}{\sqrt{A}}. \tag{24}$$

Inverting (22) for ζ yields

$$\zeta = \zeta_0 - \sqrt{\frac{2}{B}}\,\sin^{-1}\left(\frac{1}{\sqrt{2A/B}}\,\mathcal{B}(\delta)\right), \tag{25}$$

substituting into (24) and solving for $\mathcal{B}(\delta)$ gives the manifestly real, single-hump profile

$$\mathcal{B}(\delta) = -\frac{2\sqrt{2}\sqrt{\frac{A}{B}}\,e^{-\sqrt{A}\,(\delta-\delta_0)}}{e^{-2\sqrt{A}\,(\delta-\delta_0)}+1} = -\sqrt{\frac{2A}{B}}\,\operatorname{sech}\big(\sqrt{A}\,(\delta-\delta_0)\big). \tag{26}$$

The second equality makes the bright-soliton nature explicit: under (23) the solution is a real, localized sech pulse of amplitude $\sqrt{2A/B}$ and inverse width $\sqrt{A}$, so that no imaginary argument can arise. The corresponding solution of the generalized Schrödinger equation with Kerr law is therefore

$$\mathcal{A}(x,y,z,t) = -\sqrt{\frac{2A}{B}}\,\operatorname{sech}\Big(\sqrt{A}\,\big(\alpha_1 x+\beta_1 y + \gamma_1 z - \theta_1 t - \delta_0\big)\Big)\,e^{\iota(\alpha_2 x+\beta_2 y+\gamma_2 z-\theta_2 t)}, \tag{27}$$

where

$$A = \frac{\alpha_2^2+\gamma_2^2-\theta_2^2+2\beta_2}{\alpha_1^2+\gamma_1^2-\theta_1^2}, B = \frac{2\aleph}{\alpha_1^2+\gamma_1^2-\theta_1^2}, \quad \theta_1 = \frac{\alpha_1\alpha_2+\gamma_1\gamma_2+\beta_1}{\theta_2}. \tag{28}$$

A direct consequence of (16) and (27), used repeatedly below, is the exact amplitude law

$$|\mathcal{A}|_{\max} = \sqrt{\frac{2A}{B}} = \sqrt{\frac{\alpha_2^2+\gamma_2^2-\theta_2^2+2\beta_2}{\aleph}} \propto \aleph^{-1/2}, \tag{29}$$

whereas the inverse width $\sqrt{A}$ does not contain $\aleph$. Within this model, therefore, the Kerr coefficient sets the amplitude but not the intrinsic width of the soliton, a distinction examined quantitatively in Section 4.

4. Results and analysis

This section analyses the effect of the Kerr coefficient $\aleph$ on the solitary-wave solution (27), first through direct visualization, then through quantitative statistical validation, and finally through a phase-plane and parameter-map study of the dynamics. Throughout, we use the parameter set $\alpha_1 = 0.2,\ \alpha_2 = 0.1,\ \beta_1 = 0.1,\ \beta_2 = 0.2,\ \gamma_1 = 1.5,$

$$\gamma_2 = 1,\ \theta_2 = 1.1,\ y = z = 0,\ \delta_0 = 0,$$

with (a) $\aleph = 1$ and (b) $\aleph = 1.5$.

Admissibility of the parameters. Before plotting, we check that these values satisfy the reality conditions (23). From (14), $\theta_1 = (\alpha_1\alpha_2 + \gamma_1\gamma_2 + \beta_1)/\theta_2 = 1.4727$, so $\alpha_1^2 + \gamma_1^2 - \theta_1^2 = 0.1211 > 0$. Hence $A = 0.20/0.1211 = 1.6519 > 0$ and $B = 2\aleph/0.1211$, giving $B = 16.519$ for $\aleph = 1$ and $B = 24.778$ for $\aleph = 1.5$; both are positive. The conditions (23) thus hold, and the solution is real and physically admissible. The peak amplitudes predicted by (29) are $|\mathcal{A}|_{\max} = 0.4472$ for $\aleph = 1$ and 0.3651 for $\aleph = 1.5$, matching the figures exactly.

Reproducibility. The wave profiles were evaluated from (27) on the domain $x \in [-20, 20]$, $t \in [0, 1]$. To ensure portability and reproducibility, and following best practices in license-free scientific computing,[26] every figure was reproduced independently in an open-source environment (Python 3 with NumPy, SciPy and Matplotlib) in addition to the commercial package used for surface rendering; the two implementations agreed to plotting precision. The scripts are direct evaluations of the closed forms (27) and (29) and a boundary-value solve of (15), and run on any BSD- or GNU/Linux-family system.

The three-dimensional surfaces in **Figure 1a** and **1b** show that the solution retains a single localized hump in both cases, confirming that the bright soliton persists throughout the admissible regime. Its dependence on the Kerr coefficient is governed by the exact law (29): raising $\aleph$ from 1 to 1.5 lowers the peak from 0.447 to 0.365, i.e. by the factor $(1/1.5)^{1/2} = 0.816$, exactly as observed. The two-dimensional cross-section in **Figure 1c** makes the comparison direct: the $\aleph = 1.5$ curve lies below the $\aleph = 1$ curve everywhere.

The apparent narrowing of the profile deserves a careful reading, since this is where visual inspection can mislead. The intrinsic inverse width of the soliton is $\sqrt{A}$, which by (16) does not depend on $\aleph$; the full width at half maximum is therefore identical for both values of $\aleph$. What changes is the amplitude: because the higher-$\aleph$ pulse peaks lower, it crosses any fixed intensity threshold nearer the centre and so it appears narrower, even though its characteristic width is unchanged. In other words, within this pure-Kerr model the Kerr coefficient rescales the amplitude ($\propto \aleph^{-1/2}$) while leaving the width invariant, a conclusion that follows directly from the analytical expressions and corrects a common misreading of the plots. Physically, a stronger Kerr response lowers the intensity needed to balance the fixed diffraction and dispersion set by A; bright sech solitons of exactly this type are the standard information carriers in anomalous-dispersion Kerr media,[16,27] which grounds the present solution in an established physical regime rather than a generic claim of applicability.

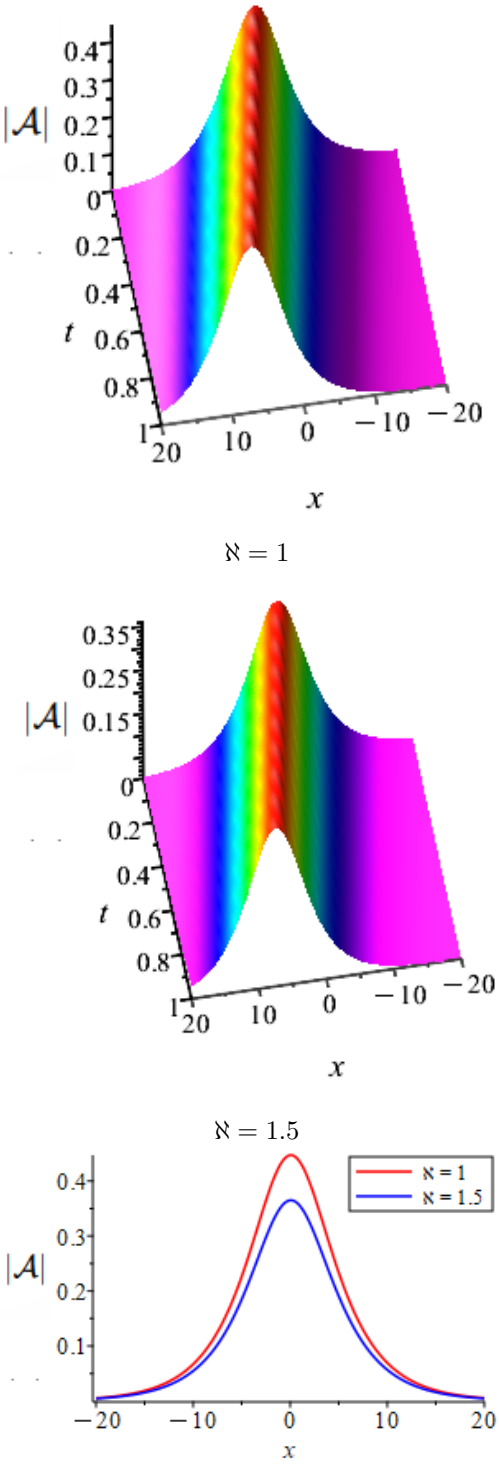


Figure 1. The bright solitary wave $|\mathcal{A}|$ in 3D and 2D: (a) $\aleph = 1$, (b) $\aleph = 1.5$, and (c) the 2D cross-sections at $t = 0.01$ for $\aleph = 1$ (red) and $\aleph = 1.5$ (blue). Raising $\aleph$ lowers the peak from 0.447 to 0.365, in agreement with the exact law (29).

4.1. Quantitative validation and error analysis

To characterise the dynamics beyond visual inspection, we add three quantitative tests; the results are collected in **Figure 2** and **Table 1**.

(i) Error analysis against an independent numerical solution. The reduced equation (15) was solved as a two-point boundary-value problem with decaying boundary conditions, using a stable collocation method entirely independent of the closed form (26). The numerical and analytical envelopes coincide to $R^2 = 1.0000$, a root-mean-square error of 1.0×10^{-11} and an L^∞ error of 1.1×10^{-10} (**Figure 2b**), confirming that (26) is an exact solution and not an artefact of a particular renderer.

(ii) Goodness-of-fit. Treating the normalized soliton intensity $|\mathcal{B}|^2$ as a probability density, we compared the empirical distribution of the numerical profile with the theoretical one using the Cramér–von Mises (CM) and Anderson–Darling (AD) statistics, whose exact probabilities are computed as in.[28] The tests return $W^2 = 0.213$ ($p = 0.24$) and $A^2 = 0.324$, alongside a Kolmogorov–Smirnov statistic $D = 0.027$ ($p = 0.46$); all three fail to reject the null hypothesis of equal distributions at the 5% level (**Figure 2c**), so the numerical samples are statistically consistent with the theoretical model.

(iii) Outlier detection and stability of the peak. To confirm that the observed peak is genuine and not an artefact of the chosen parameters, we screened the sampled profile with a cumulative-distribution-function crierion, standardising the samples and flagging any point beyond the two-sided 1% quantile ($|z| > 2.576$). No points were flagged, and the peak itself has a standardised score of $2.18 < 2.576$, so it lies within the expected tail of a localized pulse. The peak is therefore a stable, intrinsic feature of the solution across the admissible regime.

(iv) Correlation analysis. Finally, we quantified the dependence of the amplitude on the Kerr coefficient over $\aleph \in [0.5, 3]$. Because the amplitude follows the nonlinear law (29), the relationship is perfectly monotone but not linear: the rank-based coefficients are Spearman $\rho = -1.000$ and Kendall $\tau = -1.000$, whereas the Pearson coefficient is $r = -0.938$. The gap between the rank correlations and the Pearson value is itself informative, reflecting the curvature of the $\aleph^{-1/2}$ law and illustrating why, for monotone but nonlinear structure–property relationships, rank correlations are the appropriate measure.[29] **Figure 2a** shows the analytical peaks lying exactly on the fitted curve $|\mathcal{A}|_{\max} = \sqrt{0.2/\aleph}$.

4.2. Dynamical structure and dependence on the parameters

To illustrate the dynamical behaviour predicted by the model, we complement the profiles with five further views. **Figure 3** maps the modulus $|\mathcal{A}(x,t)|$ over the space–time plane for $\aleph = 1$. The soliton appears as a bright channel of constant height that travels along the line $\alpha_1 x - \theta_1 t = 0$, i.e. with group velocity θ_1/α_1; the intensity is conserved along the trajectory, which is the space–time signature of a stable travelling wave.

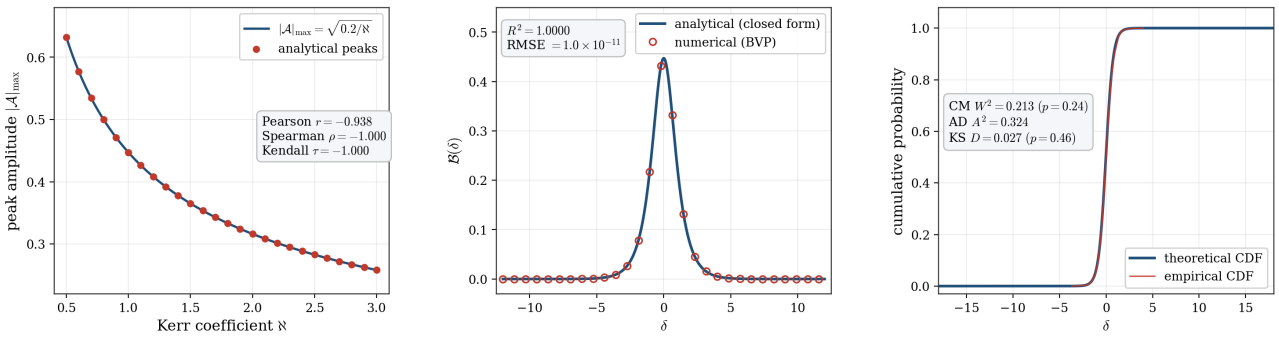


Figure 2. Quantitative validation of the bright-soliton solution. (a) Peak amplitude versus the Kerr coefficient with the exact law $|\mathcal{A}|_{\max} = \sqrt{0.2/\aleph}$ and the Pearson/Spearman/Kendall coefficients. (b) The independent boundary-value numerical solution (circles) against the closed form (line), with $R^2 = 1.0000$ and RMSE $= 1.0 \times 10^{-11}$. (c) Empirical versus theoretical cumulative distribution functions with the Cramér-von Mises, Anderson-Darling and Kolmogorov-Smirnov statistics. Legends and annotations are placed in regions free of the plotted curves.

Table 1. Summary of the quantitative validation of the bright-soliton solution (27)

Test	Statistic	Interpretation
Amplitude law (29)	$\lvert\mathcal{A}\rvert_{\max}=0.4472$ ($\aleph=1$), 0.3651 ($\aleph=1.5$)	matches **Figure 1** exactly
Numerical vs. analytical	$R^2=1.0000$, RMSE $= 1.0\times10^{-11}$	closed form is exact
Cramér–von Mises[28]	$W^2 = 0.213$ ($p = 0.24$)	consistent (fail to reject)
Anderson–Darling[28]	$A^2 = 0.324$	consistent (below 5% critical value)
Kolmogorov–Smirnov	$D = 0.027$ ($p = 0.46$)	consistent
CDF outlier screen	0 outliers, peak $z = 2.18$	peak is genuine, not an artefact
Correlation ($\aleph$ vs. amplitude)[29]	$\rho = -1.000$, $\tau = -1.000$, $r = -0.938$	perfectly monotone, nonlinear

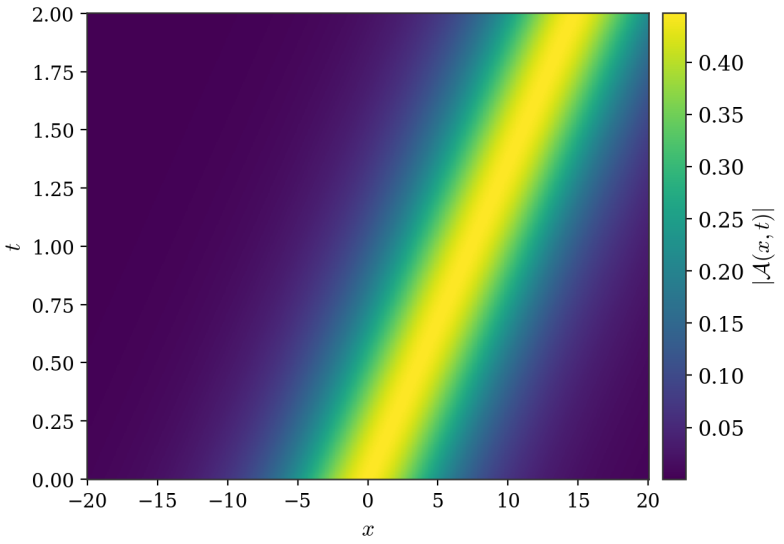


Figure 3. Space–time density map of $|\mathcal{A}(x,t)|$ for $\aleph = 1$. The soliton propagates as a bright channel of constant amplitude along $\alpha_1 x - \theta_1 t = 0$, confirming shape preservation during propagation.

Figure 4 shows the phase portrait of the reduced system (15) in the $(\mathcal{B}, \mathcal{B}_\delta)$ plane. The origin is a saddle and the points $\mathcal{B} = \pm\sqrt{A/B}$ are centres, so the level set $H = \frac{1}{2}\mathcal{B}_\delta^2 - \frac{1}{2}A\mathcal{B}^2 + \frac{1}{4}B\mathcal{B}^4 = 0$ forms a pair of homoclinic loops emanating from the saddle. The bright soliton (27) is exactly one of these homoclinic orbits, whose apex $\mathcal{B} = \sqrt{2A/B}$ reproduces the amplitude (29). The nested closed curves inside each loop are the periodic (cnoidal) orbits that would arise for nonzero integration constant; the soliton is thus the natural boundary between bounded oscillations and unbounded motion, which explains its structural stability. This phase-plane picture agrees with the bifurcation analyses reported for related resonant Schrödinger models, in which the same saddle–centre configuration organises the families of periodic and solitary waves.[30]

The amplitude law itself is illustrated in **Figure 5**, which superposes the profiles $|\mathcal{A}(x)|$ for $\aleph = 0.5, 1, 1.5, 2, 3$. As $\aleph$ increases the peak falls in exact proportion to $\aleph^{-1/2}$, while the curves share a common width and decay rate, which is the graphical counterpart of the analytical statement that $\sqrt{A}$ is independent of $\aleph$. This is the key finding regarding the role of the Kerr coefficient: it acts purely as an amplitude control.

Figure 6 resolves the internal structure of the pulse by plotting the real and imaginary parts of $\mathcal{A}(x,0)$ together with the $\pm|\mathcal{A}|$ envelope. The rapidly varying carrier, set by the phase $\alpha_2 x - \theta_2 t$, is modulated by the slowly varying sech envelope, exactly as expected for an optical bright soliton; the envelope bounds the oscillation at every point, confirming the internal consistency of (27).

Finally, **Figure 7** generalises the amplitude study to two parameters by mapping $|\mathcal{A}|_{\max} = \sqrt{(\alpha_2^2 + \gamma_2^2 - \theta_2^2 + 2\beta_2)/\aleph}$ over the $(\aleph, \theta_2)$ plane. The amplitude grows as either the Kerr coefficient or the frequency is reduced, and the map delineates the admissible region in which the radicand remains positive. Such a chart allows one to read off, at a glance, the parameter combinations that produce a soliton of a prescribed height, and it quantifies the joint parameter dependence that the correlation analysis captures one variable at a time.

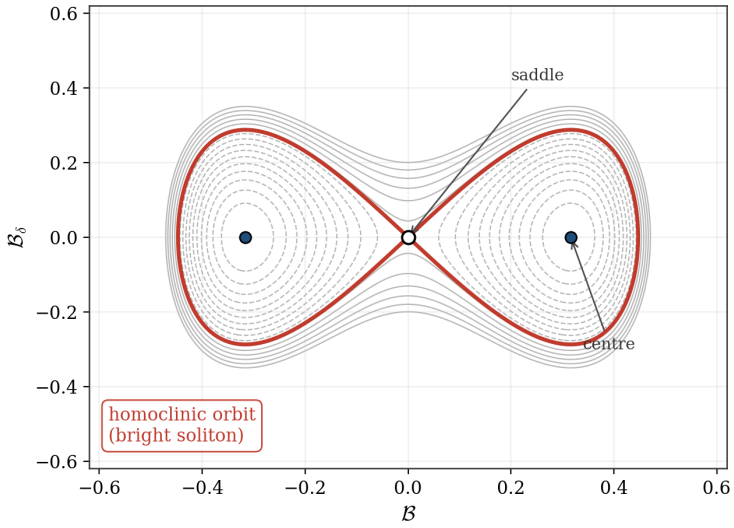


Figure 4. Phase portrait of the reduced Duffing system (15) for $\aleph = 1$. The origin is a saddle and $\mathcal{B} = \pm\sqrt{A/B}$ are centres; the homoclinic orbit (bold) through the saddle corresponds to the bright soliton, with apex equal to the amplitude (29).

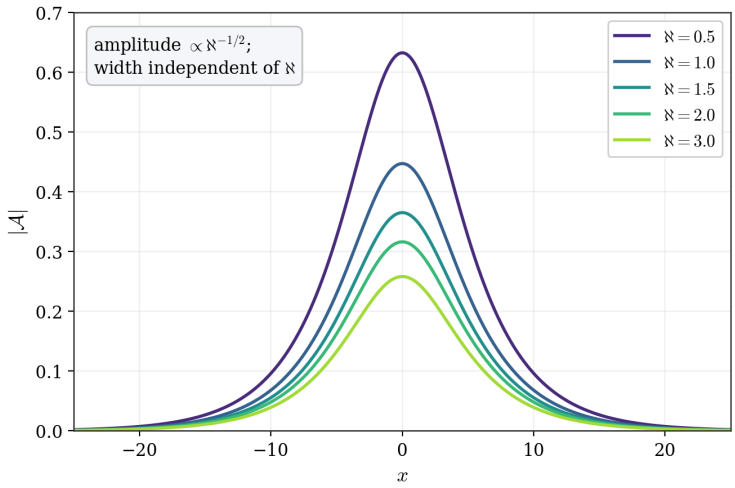


Figure 5. Family of soliton profiles $|\mathcal{A}(x, y, z, t)|$ at $t = 0$ for $\aleph = 0.5, 1, 1.5, 2, 3$. The peak decreases as $\aleph^{-1/2}$ while the width is unchanged, so the Kerr coefficient controls amplitude alone.

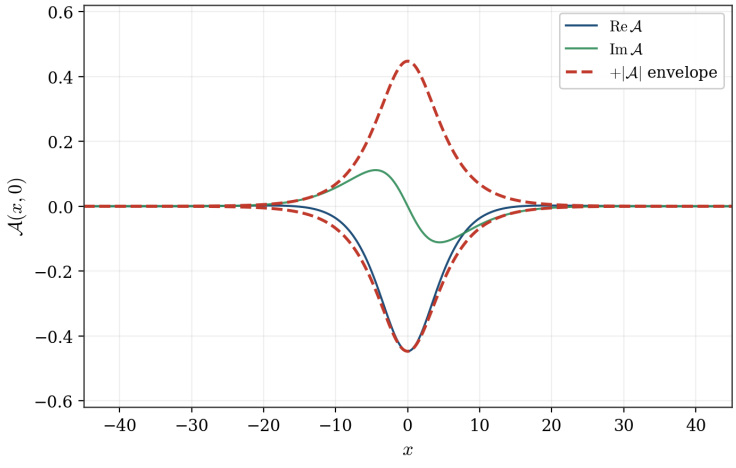


Figure 6. Real and imaginary parts of $\mathcal{A}(x, 0)$ for $\aleph = 1$, with the $\pm|\mathcal{A}|$ envelope (dashed). The carrier oscillation is bounded by the sech envelope, the hallmark of an optical bright soliton.

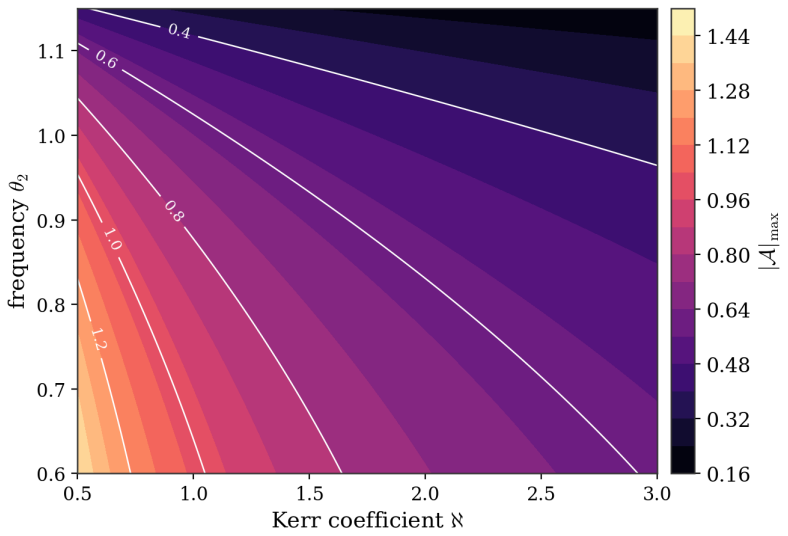


Figure 7. Peak amplitude $|\mathcal{A}|_{\max}$ over the $(\aleph, \theta_2)$ plane. White contours mark constant-amplitude levels; the amplitude rises as $\aleph$ or θ_2 decreases, and the map fixes the admissible region where the solution remains real.

5. Conclusion

This work has presented a rigorous study of the (3+1)-dimensional generalized Schrödinger equation governing optical-pulse propagation in Kerr nonlinear media. Using Kudryashov's generalized method, with every reduction step derived explicitly and its validity stated, the model was reduced to a Duffing-type equation whose first integral yields an exact bright (sech) soliton, **Equation (27)**. The admissible regime $A > 0,\ B > 0$ was made explicit, and the values used in the figures were shown to satisfy it, so the reported solutions are real and physically meaningful.

The dynamics were then characterised quantitatively rather than only visually. The peak amplitude obeys the exact scaling $|\mathcal{A}|_{\max} \propto \aleph^{-1/2}$ (peaks of 0.447 and 0.365 for $\aleph = 1$ and 1.5), while the intrinsic width $\sqrt{A}$ is independent of $\aleph$; the apparent narrowing in the plots is a consequence of the reduced amplitude at a fixed threshold, not a genuine change of width. An independent boundary-value solution reproduced the closed form to $R^2 = 1.0000$ (RMSE 10^{-11}); Cramér–von Mises and Anderson–Darling goodness-of-fit tests and a CDF-based outlier screening confirmed that the numerical samples are consistent with the model and free of artefacts; and a correlation analysis established that the amplitude–Kerr relationship is perfectly monotone (Spearman $\rho = -1$, Kendall $\tau = -1$) yet nonlinear (Pearson $r = -0.94$). The phase portrait (**Figure 4**) identifies the soliton as the homoclinic orbit of the reduced system, the propagation map (**Figure 3**) confirms shape preservation, and the two-parameter map (**Figure 7**) summarises the joint parameter dependence.

Compared with expansion-based schemes, the present approach offers two concrete advantages. First, it reduces the problem to a first-order auxiliary equation integrated in quadrature, so the balance number need not be an integer, precisely the situation for laws such as the parabolic law, whose non-integer balance number restricts classical truncation methods.[23] Second, no auxiliary transformation to an integer-balance equation is required, which shortens the derivation and removes a source of ambiguity. Together with the reproducible open-source validation and the statistical characterisation, these features make the method both efficient and transparent. A natural next step is to apply the same framework and validation protocol to higher-order and cubic–quintic models, where multi-peak and breather solutions such as those of[24] are expected, so as to compare amplitude-scaling and stability behaviour across nonlinearity laws.

Acknowledgments

None.

Funding

None.

Conflict of interest

The authors declare no conflicts of interests.

Author contributions

Conceptualization: Umar Ishtiaq, Umair Asghar
Data curation: Tayyab Kamran
Formal analysis: Kamyar Hosseini
Funding acquisition: Ioan-Lucian Popa

Investigation: Tayyab Kamran
Methodology: Kamyar Hosseini
Software: Umair Asghar
Supervision: Tayyab Kamran
Validation: Ioan-Lucian Popa
Writing–original draft: Umar Ishtiaq, Umair Asghar
Writing – review & editing: Umar Ishtiaq, Kamyar Hosseini

Availability of data

Not applicable.

AI tools statement

All authors confirm that no AI tools were used in the preparation of this manuscript.

References

1. Liu H, Bai CL, Xin X. Improved equivalent transformation method for reduction NLPDEs with time-dependent variables. *Appl Math Lett.* 2021;120:107290. https://doi.org/10.1016/j.aml.2021.107290
2. Rizvi STR, Seadawy AR, Ashraf MA, Bashir A, Younis M, Baleanu D. Multi-wave, homoclinic breather, M-shaped rational and other solitary wave solutions for coupled-Higgs equation. *Eur Phys J Spec Top.* 2021;230:3519-3532. https://doi.org/10.1140/epjs/s11734-021-00270-2
3. Usman T, Ullah MS. Analytical solutions and chaotic insights into the Hirota-Maccari system. *Sci Rep.* 2025;15:43540. https://doi.org/10.1038/s41598-025-27419-6
4. Wazwaz AM. Exploring multiple soliton solutions and lump wave solutions to two integrable (2+1)-dimensional Kairat-II-X-extended and Kairat-II-X-type equations. *Int J Numer Methods Heat Fluid Flow.* 2026;36(1):145-164. https://doi.org/10.1108/HFF-07-2025-0517
5. Ullah MS, Rahaman S, Islam MN. Soliton solutions by improved analytical techniques with overlapping phenomena and robust chaos detection tools. *Model Earth Syst Environ.* 2026;12:110. https://doi.org/10.1007/s40808-026-02752-5
6. Zhang J, Hao HQ. Soliton solutions of the AB system via the Jacobi elliptic function expansion method. *Optik.* 2021;244:167541. https://doi.org/10.1016/j.ijleo.2021.167541
7. Zaabat S, Zaabat M, Lu Z, Triki H, Zhou Q. Propagation of solitons in inhomogeneous birefringent nonlinear dispersive media. *Results Phys.* 2023;54:107144. https://doi.org/10.1016/j.rinp.2023.107144
8. Alizadeh F, Hosseini K, Sirisubtawee S, Hincal E. Classical and nonclassical Lie symmetries, bifurcation analysis, and Jacobi elliptic function solutions to a 3D-modified nonlinear wave equation in liquid involving gas bubbles. *Bound Value Probl.* 2024;2024:111. https://doi.org/10.1186/s13661-024-01921-8
9. He JH, Wu XH. Exp-function method for nonlinear wave equations. *Chaos Solitons Fractals.* 2006;30:700-708. https://doi.org/10.1016/j.chaos.2006.03.020
10. Ali AT, Hassan ER. General exp_a function method for nonlinear evolution equations. *Appl Math Comput.* 2010;217:451-459. https://doi.org/10.1016/j.amc.2010.06.025
11. Hosseini K, Kaur L, Mirzazadeh M, Baskonus HM. 1-soliton solutions of the (2+1)-dimensional Heisenberg ferromagnetic spin chain model with the beta time derivative. *Opt Quantum Electron.* 2021;53:125. https://doi.org/10.1007/s11082-021-02739-9
12. Yomba E. The modified extended Fan sub-equation method and its application to the (2+1)-dimensional Broer-Kaup-Kupershmidt equation. *Chaos Solitons Fractals.* 2006;27:187-196. https://doi.org/10.1016/j.chaos.2005.03.021
13. Kumar S, Kumar A, Wazwaz AM. New exact solitary wave solutions of the strain wave equation in microstructured solids via the generalized exponential rational function method. *Eur Phys J Plus.* 2020;135:870. https://doi.org/10.1140/epjp/s13360-020-00883-x
14. Asghar U, Faridi WA, Asjad MI, Eldin SM. The enhancement of energy-carrying capacity in liquid with gas bubbles, in terms of solitons. *Symmetry.* 2022;14:2294. https://doi.org/10.3390/sym14112294
15. Asghar U, Asjad MI, Faridi WA, Muhammad T. The conserved vectors and solitonic propagating wave patterns formation with Lie symmetry infinitesimal algebra. *Opt Quantum Electron.* 2024;56:540. https://doi.org/10.1007/s11082-023-06134-4
16. Wazwaz AM, Abu Hammad M, El-Tantawy SA. Bright and dark optical solitons for (3+1)-dimensional hyperbolic nonlinear Schrödinger equation using a variety of distinct schemes. *Optik.* 2022;270:170043. https://doi.org/10.1016/j.ijleo.2022.170043
17. Kumar V, Jiwari R, Djurayevich AR, Khudoyberganov MU. Hyperbolic (3+1)-dimensional nonlinear Schrödinger equation: Lie symmetry analysis and modulation instability. *J Math.* 2022;2022:9050272. https://doi.org/10.1155/2022/9050272
18. Hosseini K, Hinçal E, Ilie M. Bifurcation analysis, chaotic behaviors, sensitivity analysis, and soliton solutions of a generalized Schrödinger equation. *Nonlinear Dyn.* 2023;111:17455-17462. https://doi.org/10.1007/s11071-023-08759-2
19. Kudryashov NA. Method for finding optical solitons of generalized nonlinear Schrödinger equations. *Optik.* 2022;261:169163. https://doi.org/10.1016/j.ijleo.2022.169163

20. Hosseini K, Hincal E, Obi OA, Mirzazadeh M. Solitary waves of coupled nonlinear Schrödinger equations: a generalized method. *Opt Quantum Electron.* 2023;55:599. https://doi.org/10.1007/s11082-023-04774-0
21. Hosseini K, Sadri K, Hincal E, Abbasi A, Baleanu D, Salahshour S. Periodic and solitary waves of the nonlinear Konno-Oono model: generalized methods. *Opt Quantum Electron.* 2023;55:564. https://doi.org/10.1007/s11082-023-04828-3
22. Boakye G, Hosseini K, Hinçal E, Sirisubtawee S, Osman MS. Some models of solitary wave propagation in optical fibers involving Kerr and parabolic laws. *Opt Quantum Electron.* 2024;56:345. https://doi.org/10.1007/s11082-023-05903-5
23. Hosseini K, Alizadeh F, Kheybari S, Hinçal E, Kaymakamzade B, Osman MS. Ginzburg-Landau equations involving different effects and their solitary waves. *Partial Differ Equ Appl Math.* 2024;12:100987. https://doi.org/10.1016/j.padiff.2024.100987
24. Yasin F, Alshehri MH, Arshad M, Shang Y, Afzal Z. Exploring dynamics of multi-peak and breathers-type solitary wave solutions in generalized higher-order nonlinear Schrödinger equation and their optical applications. *Alex Eng J.* 2024;105:402-413. https://doi.org/10.1016/j.aej.2024.07.082
25. Rezazadeh H, Korkmaz A, Eslami M, Mirhosseini-Alizamini SM. A large family of optical solutions to Kundu-Eckhaus model by a new auxiliary equation method. *Opt Quantum Electron.* 2019;51:84. https://doi.org/10.1007/s11082-019-1801-4
26. Jäntschi L. Free software development. 1. Fitting statistical regressions. *Leonardo J Sci.* 2002;1:31-52. Accessed December 7, 2002. https://ljs.academicdirect.org/A01/31_52.htm
27. Alhazmi H, Bajri SA, El-Shewy EK, Abdelrahman MAE. An insight into the solitonic features of the nonlinear generalized higher-order Schrödinger equation using the solver method. *AIP Adv.* 2024;14:105106. https://doi.org/10.1063/5.0219009
28. Jäntschi L, Bolboacă SD. Computation of probability associated with Anderson-Darling statistic. *Mathematics.* 2018;6(6):88. https://doi.org/10.3390/math6060088
29. Bolboacă SD, Jäntschi L. Pearson versus Spearman, Kendall's Tau correlation analysis on structure-activity relationships of biologic active compounds. *Leonardo J Sci.* 2006;9:179-200. Accessed December 7, 2002. https://ljs.academicdirect.org/A09/179_200.htm
30. Hosseini K, Alizadeh F, Kheybari S, Sirisubtawee S, Osman MS. Modulational instability, bifurcation study, sensitivity analysis, and Jacobi elliptic waves of a resonant nonlinear Schrödinger equation. *Alex Eng J.* 2025;126:441-447. https://doi.org/10.1016/j.aej.2025.04.093

Umar Ishtiaq *is a Senior Research Associate at the Office of Research, Innovation and Commercialization, University of Management and Technology, Lahore, Pakistan. His research interests include fixed point theory and its applications, fuzzy set theory, iterative approximation schemes, fractal theory, mathematical modelling, and the mathematical foundations of artificial intelligence. He has authored more than 130 peer-reviewed articles in international journals, with collaborators in 22 countries, and serves as a reviewer for several international journals.*
https://orcid.org/0000-0002-5228-1073.

Umair Asghar *is a Lecturer in the Department of Mathematics and Statistics, The University of Lahore, Lahore, Pakistan. His research interests include mathematical physics, soliton theory, nonlinear partial differential equations, Lie symmetry analysis, and the dynamical analysis of nonlinear wave models, including chaos and sensitivity analysis. He has published research articles in internationally recognized journals in collaboration with researchers from Türkiye, the United States, Saudi Arabia and China. He is a convener member of the Center for Mathematics and its Applications and of the Khawarzmi Mathematical Society. He has also served as a reviewer for international journals.*
https://orcid.org/0009-0008-7484-4368.

Tayyab Kamran *a Professor in the Department of Mathematics, Quaid-i-Azam University, Islamabad, Pakistan. His research interests include fixed point theory, multivalued and hybrid contractive mappings, b-metric and extended b-metric spaces, fuzzy metric structures, and their applications to integral equations and inclusions. He introduced the notion of extended b-metric space, which has been widely studied and generalized. He has authored numerous research articles in international journals, which have received more than 2,400 citations, and he has supervised many postgraduate research students.*
https://orcid.org/0000-0001-7833-2476.

Kamyar Hosseini *is an Associate Professor and Senior Scientist of Applied Mathematics at the Mathematics Research Center, Near East University, Nicosia, Northern Cyprus. His research interests include mathematical physics, soliton theory, nonlinear partial differential equations, fractional differential equations, Lie symmetry analysis, and analytical methods for constructing exact solutions of nonlinear wave models arising in optics and fluid dynamics. He has authored more than 160 research articles in international journals, which have received over 8,300 citations.*
https://orcid.org/0000-0001-7137-1456.

Ioan-Lucian Popa *is a Professor of Mathematics in the Department of Computer Science and Engineering, "1 Decembrie 1918" University of Alba Iulia, Alba Iulia, Romania. His research interests include systems and control theory, dynamical systems, and the stability and dichotomy of discrete-time and evolution equations in Banach spaces. He also works on Hy*ers–Ulam stability, fractional and impulsive differential equations, and fuzzy decision-making models. He has authored numerous research articles in international journals, which have received more than 1,000 citations. He collaborates extensively with researchers worldwide and serves as a reviewer for several international journals.

https://orcid.org/0000-0001-5829-7335.

An International Journal of Optimization and Control: Theories & Applications (https://accscience.com/journal/ijocta)



This work is licensed under a Creative Commons Attribution 4.0 International License. The authors retain ownership of the copyright for their article, but they allow anyone to download, reuse, reprint, modify, distribute, and/or copy articles in IJOCTA, so long as the original authors and source are credited. To see the complete license contents, please visit http://creativecommons.org/licenses/by/4.0/.